buildings

MDPI

Article

Predicting Crack Width in CFRP-Strengthened RC One-Way Slabs Using Hybrid Grey Wolf Optimizer Neural Network Model

Seyed Vahid Razavi Tosee [1], Iman Faridmehr [2], Moncef L. Nehdi [3,*], Vagelis Plevris [4] and Kiyanets A. Valerievich [2]

[1] Department of Civil Engineering, Jundi-Shapur University of Technology, Dezful 18674-64616, Iran
[2] Department of Building Construction and Structural Theory, South Ural State University, 76 pr. Lenina, 454080 Chelyabinsk, Russia
[3] Department of Civil Engineering, McMaster University, Hamilton, ON L8S 4M6, Canada
[4] Department of Civil and Architectural Engineering, College of Engineering, Qatar University, Doha P.O. Box 2713, Qatar
* Correspondence: nehdim@mcmaster.ca

Abstract: This study deploys a hybrid Grey Wolf Optimizer Neural Network Model for predicting the crack width in reinforced concrete slabs strengthened with carbon fiber-reinforced polymers (CFRP). Reinforced concrete (RC) one-way slabs (1800 × 400 × 120 mm in size) were strengthened with CFRP with various lengths (1800, 1100, and 700 mm) and subjected to four-point bending. The experimental results were compared to corresponding values for conventional RC slabs. The observed crack width results were recorded, and subsequently examined against the expression recommended by Eurocode 2. To estimate the crack width of CFRP-reinforced slabs, ANN combined with the Grey Wolf Optimizer algorithm was employed whereby the applied load, CFRP width/length, X/Y crack positions, and stress in steel reinforcement and concrete were defined as the input parameters. Experimental results showed that the larger the length and width of the carbon fiber, the smaller the maximum crack width in the tensile area of the slab at the final load step. On average, the crack width in slabs retrofitted with CFRP laminates increased by around 80% compared to a slab without CFRP. The results confirm that the equation provided by Eurocode 2 provides an unconservative estimation of crack widths for RC slabs strengthened with CFRP laminates. On the other hand, the results also confirm that the proposed informational model could be used as a reliable tool for estimating the crack width in RC slabs. The findings provide valuable insight into the design approaches for RC slabs and rehabilitation strategies for existing deficient RC slabs using CFRP.

Keywords: crack width; CFRP; artificial intelligence; neural networks; concrete slab

Citation: Razavi Tosee, S.V.; Faridmehr, I.; Nehdi, M.L.; Plevris, V.; Valerievich, K.A. Predicting Crack Width in CFRP-Strengthened RC One-Way Slabs Using Hybrid Grey Wolf Optimizer Neural Network Model. *Buildings* **2022**, *12*, 1870. https://doi.org/10.3390/buildings12111870

Academic Editor: Andreas Lampropoulos

Received: 11 September 2022
Accepted: 1 November 2022
Published: 3 November 2022

1. Introduction

Reinforced concrete (RC) flat slabs are two-way reinforced horizontal structural elements that carry relatively light floor loads and transfer them to the structure's columns without the use of beams or girders. It is a favorable construction system offering several benefits, including (i) reducing the building height; (ii) flexibility in the design layout; (iii) decreasing the construction cost and time; and (iv) ease of installation of the electrical and mechanical networks.

Cracking of concrete generally occurs when the tensile strength of concrete is exceeded. This is inevitable in conventional RC flat slabs; once formed, the cracks will be pertinent to the slab's service lifetime. Since the cracks influence the serviceability of the slab, the limit state of excessive crack width needs to be considered in the design. Concrete may crack early in the load history. Most of the cracks in concrete initiate as a result of the following conditions:

i. Volumetric change due to plastic, autogenous, and drying shrinkage, creep under sustained load, thermal stresses at elevated temperatures, and chemical incompatibility of concrete components.
ii. Direct stresses caused by applied loads or reactions, or internal stresses caused by continuity, reversible fatigue load, long-term deflection, camber in pre-stressed systems, and environmental effects, including differential movement in structural systems.
iii. Flexural stress caused by bending.

The development of cracking in RC members by flexural or tension actions is a complex topic. A one-way slab is characterized by bending mainly in one direction, while a two-way slab is characterized by significant bending in two normally orthogonal directions. Most common RC floors belong to the two-way slab category, including wide slabs subjected to dominantly concentrated loads or rectangular slabs supported on all four edges by beams or walls with an aspect ratio of less than two. Complex behavioral issues, such as torsional effects, will cause the flexural cracking in certain regions of a two-way RC slab to be different from that in one-way beams or slabs. Nawy [1] considered reinforcement spacing as the most important parameter to be considered for controlling cracking in two-way slabs. He argued that the concrete cover is normally small and not a major parameter. He recommended that the maximum spacing of the reinforcement in both orthogonal directions, in the form of either individual steel bars or mesh, should not exceed 300 mm in any slab. Moreover, some controversy exists about using crack width formulas derived from tests. Nawy [2] recommended using a different equation than the well-known Gergely–Lutz equation (on which ACI 318 is based) to calculate crack widths in beams and one-way slabs [3,4]. Park and Gamble [5] explained that the Gergely–Lutz equation [6] is reliable for two-way slabs where critical cracking takes place mainly in the negative moment regions above the faces of the beams in slab and beam floors and near the columns in flat slabs, while the studies of two-way slabs reported by Nawy et al. [1] considered primarily positive moment regions. The simplified design rules for crack control in major international standards, including Eurocode 2 [7], concern a minimum reinforcement area and a limitation on bar diameter or bar spacing, depending on the magnitude of the steel stress under the service loads.

In recent decades, several studies have examined strengthening concrete flat slabs with FRP composite laminates. Mosallam and Mosalam [8] developed an experimental and analytical investigation procedure for evaluating the ultimate response of unreinforced and reinforced concrete slabs repaired and retrofitted with FRP composite strips. They concluded that FRP systems effectively increased the strength of the repaired slabs to approximately five times that of the "as-built" slabs. The potential use of a mechanically anchored un-bonded fiber-reinforced polymer (MA-UFRP) system to upgrade RC slabs deficient in flexural strength was examined by El Maaddawy and Soudki [9]. It was concluded that the MA-UFRP system resulted in up to 43% enhancement in the slab flexural strength. An innovative strengthening method combining FRP and steel materials was explored by Zheng et al. [10], in which carbon fiber laminates and thin steel plates were combined in different ways to determine the most effective hybrid strengthening configuration. Chen and Chen [11] investigated the structural behavior and punching shear strength of concrete slab–column connections strengthened with carbon fiber-reinforced polymer (CFRP) laminates. They concluded that the CFRP laminates effectively increased the punching shear strength of slab–column connections. Meanwhile, recent advances in polymer technology permitted the development of new generations of FRP rebars, such as glass fiber–reinforced polymer (GFRP) bars designated with a high modulus of elasticity. This innovative material has provided additional opportunities to increase construction productivity, enhance structural performance, reduce structure maintenance costs, and extend the RC structure service life [12,13].

Artificial neural networks (ANNs) combined with other metaheuristic algorithms have been used for universal function approximation and employed in various engineering problems of different natures [14–16]. ANNs are inspired by and based on the neural

structure of the biological brain. They can establish a functional relationship between two datasets over the learning process and replicate that relationship over a recall process. An ANN comprises an adaptable methodology that can accurately estimate highly non-linear functions over the entire domain with adequate precision. Mangalathu et al. [17] studied several machine learning methodologies (support vector regression, ridge regression, random forest, decision tree, K-nearest neighbors, adaptive boosting, and extreme gradient boosting) for estimating the punching shear strength of flat slabs and identifying the most reliable tool. The study concluded that the extreme gradient boosting model provided the lowest mean square error and the highest coefficient of determination among the examined machine learning methodologies.

ANN predictive models have been applied to many problems in economics, engineering and other scientific fields. Particularly in structural engineering [18,19] and concrete structures, they have been successfully used for predicting the compressive strength of concrete containing recycled aggregate [20,21], predicting the compressive strength of cement replacement material (CRM) samples [22], determining the nominal shear capacity of steel fiber-reinforced concrete beams [23], predicting the capacity of concrete walls [24], predicting the compressive strength of lightweight foamed concrete [25], predicting the properties of FRP-confined concrete cylinders [26], designing reinforced concrete footings [27], analyzing the vulnerability of large concrete dams [28], measuring the mechanical properties of hybrid concrete through image processing [29], and predicting the creep and shrinkage deflection of reinforced concrete beams containing GGBFS [30], among other interesting and innovative applications [31,32].

Even though several design models have been proposed to estimate the crack width of RC flat slabs, such formulas are still perceived as a work-in-progress, especially for slabs reinforced with FRP laminates. While FRP laminates can benefit a RC flat slab in terms of enhanced sectional strength and long-term durability, the uncertainty regarding their mechanical properties remains a hurdle in guaranteeing the reliability of pertinent crack width equations. For instance, most available equations are either empirical, based on fitting the available test data, or are based on the modification of existing design code estimations for steel-reinforced RC slabs by considering the lower elastic modulus of FRP laminates. Nevertheless, the accuracy of the above-mentioned approaches is still questionable due to the differences in the mechanical properties and structural behavior between FRP and conventional steel reinforcement. As documented by several researchers, FRP laminates exhibit a fragile linear elastic response and different bond characteristics, resulting in different cracking behavior than conventional steel reinforcement [33–35].

The present study aims at developing a generalized informational model for determining the crack width of RC flat slabs reinforced with FRP laminates. Unlike existing empirical equations developed based on well-established fundamental mechanical theories using geometric and material properties, the proposed comprehensive informational model can inherently and effectively capture the underlying mechanisms of cracks in RC flat slabs. Using an informational model, the information about the underlying mechanisms of crack behavior is directly extracted from existing experimental datasets and is embedded in neural networks. This implies that the informational model does not need a pre-defined mathematical expression, in contrast with existing empirical equations. Considering the complexity of crack behavior, the proposed model can offer a reliable alternative approach. Its primary advantage lies in its ability to infer a general rule from the experimental dataset with greater efficiency than developing closed mathematical equations that, in some cases, may be impractical. To this end, by retrieving pertinent experimental results reported in the open literature, an experimental database was developed, which is representative of a large proportion of RC slabs (either with FRP or conventional steel reinforcement) under pure bending test conditions. Direct comparisons with existing theoretical models and international standards were performed using this extensive, custom-made dataset. Subsequently, an artificial neural network model was developed, coupled with a meta-heuristic Grey Wolf Optimization algorithm (GWO-ANN) to form a generalized hybrid

model for estimating the crack width of RC flat slabs reinforced with FRP laminates. This model considers the key slab parameters and is designed specifically for RC flat slabs without shear reinforcement. The accuracy of the proposed informational model versus that of existing empirical equations was further examined using several statistical metrics to ensure the model's robustness and reliability.

2. Crack Width Calculation for Concrete Flat Slabs

The control of surface cracking in concrete is particularly important in certain situations. The most common of these is in cases where the surface will be visible, as excessive crack widths can give an overall impression of poor quality and limit the types of floor coverings that can be successfully applied on the slab. Crack control is also essential for durability, as the cracks will provide pathways for ingressive corrosive substances into the concrete, such as water or other chemicals.

The Eurocode 2 provides engineers with two methods for controlling cracking in reinforced concrete slabs. The overall thickness of the slab can influence the design procedure. The two methods are described as follows.

i. Calculation of Crack Widths (Clause 4.4.2.4)—formulae are provided for crack width calculations which apply to both beams and slabs for a range of design situations and are applicable irrespective of the overall depth of the element;
ii. Control of Cracking without Direct Calculation (Clause 4.4.2.3)—a simplified design method is allowed, the rules for which have been derived using the crack width formulae. Minimum reinforcement areas are determined, and limits are placed on bar diameter and bar spacing. Alternatively, for slabs with an overall depth, D_s, not exceeding 200 mm subjected to bending without significant axial tension (i.e., in a state of flexure), cracking is assumed to be satisfactory if the detailing rules in Clause 5.4.3 of Eurocode 2 are satisfied.

Beeby and Narayanan [36] can be referred to for a more detailed account of the derivation of the crack width formulae in Eurocode 2.

$$W_k = \beta S_{crm} \varepsilon_{sm} \tag{1}$$

where W_k is the design crack width; β is a factor that relates the mean crack width in tests to the design value, e.g., it equals 1.7 for cracking due to direct loading; S_{crm} is the average final crack spacing; and ε_{sm} is the average difference in strain between the steel and the concrete, including the effects of bond stress, tension stiffening, concrete shrinkage, etc.

The average final crack spacing S_{crm} can be estimated using the following equation.

$$S_{crm} = 50 + \frac{K_1 K_2 d_b}{4\rho_r} \tag{2}$$

where K_1 is a factor that takes account of the bar bond properties (0.8 is specified in Eurocode 2); K_2 is a factor that takes account of the form of the stress distribution (0.5 for pure bending); and ρ_r is the effective reinforcement ratio of the slab.

The average strain, ε_{sm}, is calculated at the section being considered, as

$$\varepsilon_{sm} = \frac{f_s}{E_s}\left[1 - \beta_1 \beta_2 \left(\frac{f_{sr}}{f_s}\right)^2\right] \tag{3}$$

where f_s is the stress in the tension steel under the serviceability condition (calculated on the basis of a cracked section); f_{sr} is the stress in the tension steel under the relevant condition that just causes the tensile strength of the concrete to be reached (calculated on the basis of a cracked section); β_1 is a factor that accounts for the bond properties of the reinforcement (1.0 for deformed bars); and β_2 is a factor that accounts for repeated stressing of the bars (0.5 for repeated stressing as the normal design situation).

The minimum area of reinforcement placed at the cross-section being designed is given by Equation (4), as a basic requirement of the design rules of Eurocode 2 for controlling cracking without requiring a direct calculation.

$$A_{st.min} = \frac{K_4 f_t A_{ct}}{f_s} \quad (4)$$

where $K_4 = \frac{z_t}{A_{ct} z}$; f_t is the mean value of the tensile strength of concrete at the critical time when the cracks might occur (a value of 3.0 MPa is recommended in Eurocode 2 for normal use); and A_{ct} is the concrete area in the tensile zone at the section of concern before cracking.

Considering a simple rectangular slab, ignoring the presence of reinforcement when calculating z_t and A_{ct}, i.e., $z_t = bD^2/6$ and $A_{ct} = bD/2$, and assuming $z = 0.8D$ gives $K_4 = 0.42$. This explains the value of 0.4 given in Eurocode 2.

Meanwhile, the simplified design rules in Eurocode 2 are based on choosing an appropriate bar diameter or bar spacing. Design engineers usually prefer this approach rather than having to calculate the crack width directly. Limits are placed on bar diameters and bar spacing to ensure that the crack widths will not generally exceed 0.3 mm for reinforced concrete elements, as shown in Table 1.

Table 1. Limitations of bar diameters and bar spacing set by Eurocode 2 to limit cracks.

Steel Stress (f_s) (MPa)	Maximum Bar Diameter (d_b) (mm)	Maximum Spacing—Pure Bending (mm)
360	10	50
320	12	100
280	16	150
240	20	200
200	25	250
160	32	300

3. Material and Methods

This section describes the characteristics of the materials utilized in this research work as well as the experimental program employed to collect data for developing the informational model.

3.1. Materials

3.1.1. Cement

ASTM C150 Type I Ordinary Portland Cement (OPC), produced from a single source with a specific surface of 3310 cm^2/g and a relative density of 1.44 g/cm^3, was utilized for all mixed materials. Table 2 shows the chemical properties of used OPC.

Table 2. Ordinary Portland cement chemical composition [37].

Oxide Composition	CaO	SiO_2	Al_2O_3	Fe_2O_3	MgO	SO_3	K_2O	Na_2O	LOI
%	63.4	19.8	5.1	3.1	2.5	2.4	1	0.19	1.8

3.1.2. Water

Potable water, free from chemical contaminants, was used for both mixing and curing. It satisfies the requirements of BS 8110 (BS, 1997) [38].

3.1.3. Fine and Coarse Aggregates

The mining sand utilized in this study was sieved to a particle size range of 0.15 mm to 2.36 mm. The fine aggregate specific gravity in the saturated surface dry state was 2.61.

In addition, crushed granite with a maximum size of 19 mm and a relative density of 2.65 was employed as the coarse material in this study. Figure 1 depicts the sand and coarse aggregate sieve analyses.

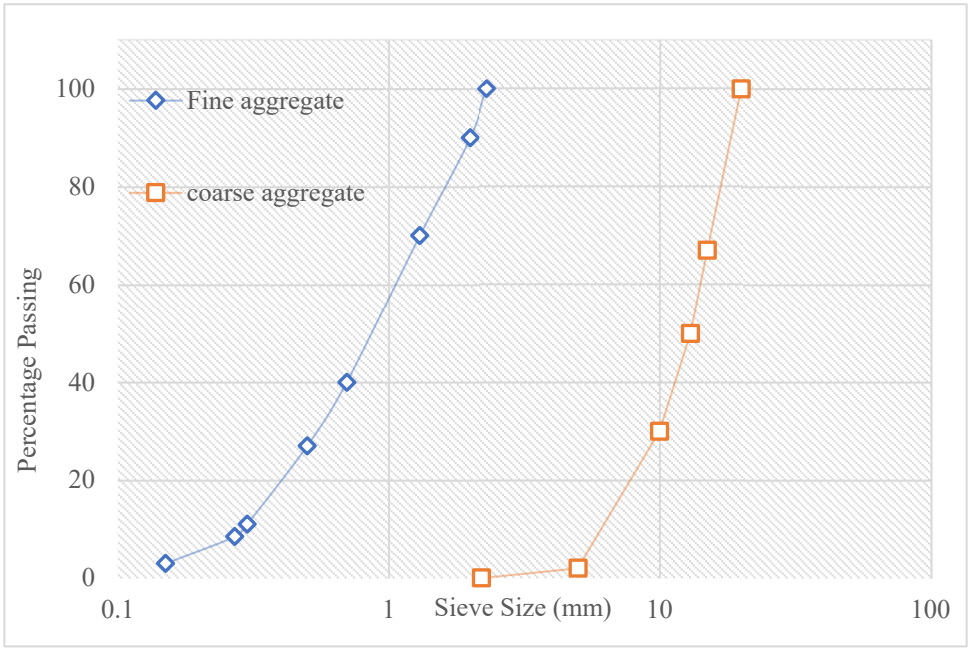

Figure 1. Distribution of particle-size of the coarse and fine aggregates.

3.1.4. Carbon Fiber-Reinforced Polymer

CFRP is composed of carbon atoms and is encased in an extremely thin fiber with a diameter of 0.005–0.010 mm. CFRP has a high strength/weight ratio, good fatigue performance, and good electrochemical corrosion resistance, making it ideal for concrete structural applications [39]. It is commonly utilized in applications that require both strong mechanical characteristics and minimal weight. Sika's pultruded carbon fiber-reinforced polymer laminates were utilized in this study to enhance the flexural performance of flat concrete slabs. Table 3 presents the mechanical characteristics of the CFRP laminate provided by the manufacturer.

Table 3. CFRP laminate mechanical characteristics.

Laminate Type	Elastic Modulus [GPa]	Tensile Strength [MPa]	Failure Strain [%]
Sika CarboDur Plates	165	3100	1.7

3.1.5. Adhesive

The Sikadur-30 adhesive from Sika was used to attach the CFRP to the RC slab. It is made of epoxy resins and a specific filler and is intended for usage at typical temperatures ranging from 8 °C to 35 °C. Table 4 shows the mechanical characteristics of the adhesive Sikadur-30 utilized in this study.

Table 4. Adhesive mechanical characteristics.

Adhesive Type	Service Temperature	Elastic Modulus [GPa]	Tensile Strength [MPa] (7 Days Curing)	
			Curing at +15 °C	Curing at +35 °C
Sikadur-30	−40 °C to +45 °C (when cured at >+23 °C)	11.2 (at +23 °C)	24–27	26–31

3.2. Concrete Mixture Design and Preparation

Concrete mix design calculates the proportions of the concrete components to obtain the required characteristics for performance and cost-efficiency. The design of experiments (DOE technique) provided by the British Department of the Environment [40] was utilized in the experimental mix design. The calculated concrete materials were combined, and the concrete specimens were cast and put under appropriate curing conditions. The tensile strength, compressive strength, and modulus of elasticity of all developed mixes were calculated based on the standards listed in Table 5. Table 6 summarizes the fresh and mechanical property test results for all tested slabs. Figure 2 shows the stress–strain curve of all tested specimens.

Table 5. Pertinent standards for examining the mechanical properties of concrete.

Test and Its Relevant Standards	Specimens and Size	Age of Testing (Day)
Compressive strength BS EN 12390-3:2002	Cubes of 100 mm	7 and 28
Splitting tensile strength BS EN 1390-6:2000	Cylinder of 150 mm diameter × 300 mm height	28
Modules of elasticity BS EN 1881-121:1983	Cylinder of 150 mm diameter × 300 mm height	28

Table 6. Fresh and hardened properties of concrete samples.

Slab Code	Slump (mm)	Compressive Strength (MPa)	Tensile Strength (MPa)	Modulus of Elasticity (MPa)
S512-700	40	46	6.8	25,842
S512-1100	41	47	5.5	28,101
S512-1500	44	42	6.3	25,963
S812-700	46	41	5.9	26,028
S812-1100	44	47	5.7	24,567
S812-1500	40	49	6.8	26,789
WCFRP	42	46	6.4	23,879
Mean Value		45	6.2	25,880

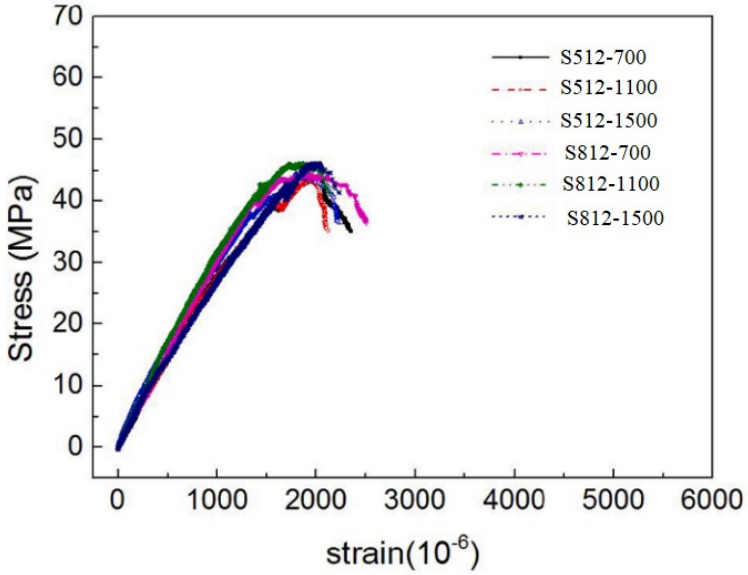

Figure 2. Stress–strain curve for all tested specimens.

3.3. Test Rig

3.3.1. Formwork

Figure 3 shows the wooden formwork constructed for the specimen casting. The internal dimensions of the formwork were 400 mm wide and 120 mm thick, while the length varied at 860, 1350, 1800, and 2400 mm. All the formwork was coated with form-release oil to achieve easier specimen removal after the concrete casting and curing.

Figure 3. Illustration of wooden formwork for concrete specimen casting.

3.3.2. Reinforcing Bar and Concrete Casting

The one-way RC slabs (either strengthened with CFRP or conventional non-strengthened ones) were reinforced longitudinally with 10 mm-diameter hot-rolled high-tensile strength deformed steel bars. The steel bars' modulus of elasticity and yield strength were 215 GPa and 610 MPa, respectively. Figure 4 depicts the longitudinal reinforcement of an RC slab.

Figure 4. Longitudinal reinforcement utilized in the tested one-way RC slabs.

Before casting the concrete, the formwork's transparent cover and internal size were ensured by utilizing a 25 mm mortar block and verifying with a measuring tape, respectively. The slabs were cured in the formwork for three days after the concrete was poured. Subsequently, as shown in Figure 5, the slabs were wet gunny cured for seven days before being stored in an unregulated concrete laboratory until the testing day.

Figure 5. Schematic of casting and curing of the prepared slabs.

3.3.3. Instrumentation

The following testing equipment and instruments were deployed in the experimental program:

- Linear variable differential transducers (LVDT)

The deflection at the center of the slab was measured using an LVDT with a 50 mm maximum deflection. The LVDT was linked to a data logger, which recorded the mid-span deflection as the load increased.

- Data Logger

The measurement mid-span deflection was recorded with a data logger (TS-TDS-302).

- Handheld microscope

A portable microscope was used to measure the flexural fractures at the level of the primary steel bar. The crack-measuring microscope had a precision of 0.02 mm and offers a 40× magnification.

Six RC one-way slabs with dimensions of 1800 × 400 × 120 mm and strengthened with various lengths and widths of CFRP were evaluated and compared to equivalent samples without CFRP. All the slabs had two steel bars with a diameter of 10 mm as longitudinal

reinforcement, and the concrete cover was 25 mm. Table 7 presents the characteristics of the specimens, i.e., unique slab code, CFRP width, and CFRP length.

Table 7. Tested slabs and properties of CFRP laminates.

Slab Code	CFRP Width (mm)	CFRP Length (mm)
S512-700	50	700
S512-1100	50	1100
S512-1500	50	1500
S812-700	80	700
S812-1100	80	1100
S812-1500	80	1500
WCFRP *	-	-

* Without CFRP.

All of the prepared slabs were tested under four-point bending loading conditions. Figure 6 depicts the instrument used and the loading configuration. As shown in the figure, mechanical discs (pre-drilled stainless-steel discs) known as Demountable Mechanical (DEMEC) were glued to the concrete surface. A DEMEC strain gauge was used to measure the changes in length between the two DEMEC points.

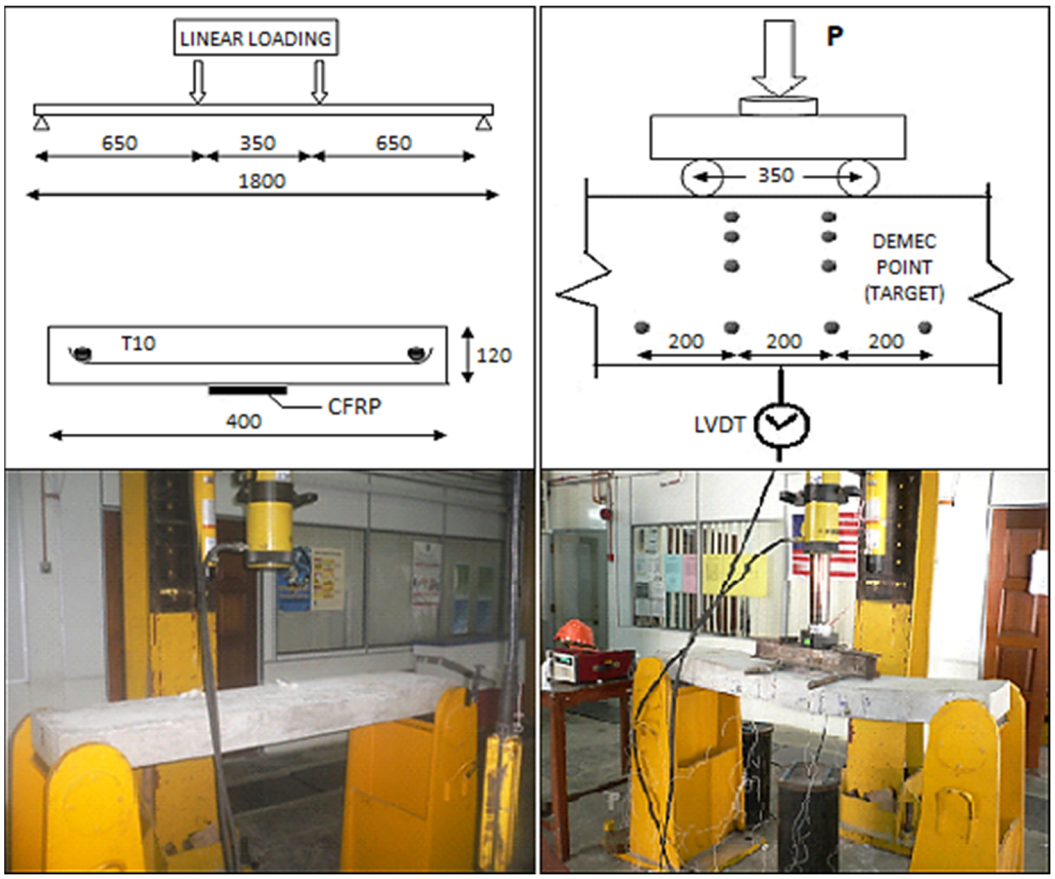

Figure 6. Instrument configuration for testing RC slabs strengthened with CFRP under linear load.

4. Experimental Results

Six CFRP-reinforced one-way RC slabs were designed, manufactured, and tested in flexure, as shown in Figure 7. All of the prepared slabs had the same shape, dimensions (width, length, depth), and internal steel reinforcement, with the width and length of the CFRP reinforcement serving as the distinguishing characteristic for each one of them. Figure 8

depicts the fracture patterns of the tested slabs. The results confirm that the steel yielding occurred prior to the collapse of the concrete in the compression zone in the slab failure mode.

Figure 7. RC slabs strengthened with CFRPs of various lengths and widths.

Figure 8. Crack pattern of RC slabs strengthened with CFRP under the four-point bending test.

As shown in Figure 9, before yielding of the steel reinforcement, the CFRP plate was de-bonded at the CFRP–concrete interface. Figure 10 shows the meticulous work of an engineer who used a portable microscope to study and quantify the flexural fractures in the CFRP-enhanced RC slabs. This was undertaken carefully at each stage of the applied stress.

Figure 9. De-bonding mechanism of concrete/CFRP interfaces under four-point bending test.

Figure 10. Crack measurement in each stage of the applied load.

The structural behavior of the RC slabs strengthened with CFRP was compared to similar benchmark slabs (in terms of materials used and dimensions), but without CFRP. For this purpose, Table 8 summarizes the bending moment at the first crack and the ultimate stage and crack width at the ultimate stage. The EC2 predicted the crack width at the service load. The results confirm the test crack width characteristics presented were reached at the post yielding load level. This behavior can be explained by the fact that attaching the CFRP laminates to the RC slabs leads to increased stiffness and bending moment capacity for the section.

Table 8. Experimental versus analytical results for estimating first crack moment and crack width.

Slab	First Crack			Ultimate Stage			
	Ex-Load (kN)	Ex-Moment (kN·m)	Anal-Moment (kN·m)	Ex-Load (kN)	Ex-Moment (kN·m)	Ex-Crack Width (mm)	EC2-Crack Width (mm)
S512-700	7.5	4.9	5.26	37	12	0.75	0.27
S512-1100	10	6.5	5.26	42	13.7	0.80	0.27
S512-1500	10	6.5	5.26	45.5	14.78	0.78	0.27
S812-700	9.5	6.2	5.45	37	12.07	0.86	0.27
S812-1100	10.3	6.7	5.45	45	14.62	0.89	0.27
S812-1500	10.5	6.8	5.45	54	17.87	0.95	0.27
WCFRP	7	4.6	4.93	33.3	10.8	0.45	0.27

The analytical first crack moment is calculated based on the following equation:

$$M_{cr} = \frac{f_{cr} I_t}{y_t} \quad (5)$$

where $f_{cr} = 0.4\sqrt{f'_c}$ (in MPa units); I_t is the moment of inertia of the transformed reinforced section (un-cracked); and y_t is the distance from the center of the un-cracked transformed section to the extreme tension fiber. Furthermore, the position and width of the fractures formed by constant moment were examined and measured over the loading protocol. Figure 11 shows the measurement reference for recording the cracks, determined using the left-hand coordinate. Tables 9–11 list the recorded crack widths and locations for RC slabs retrofitted with CFRP laminates (all six specimens) during the pure bending testing.

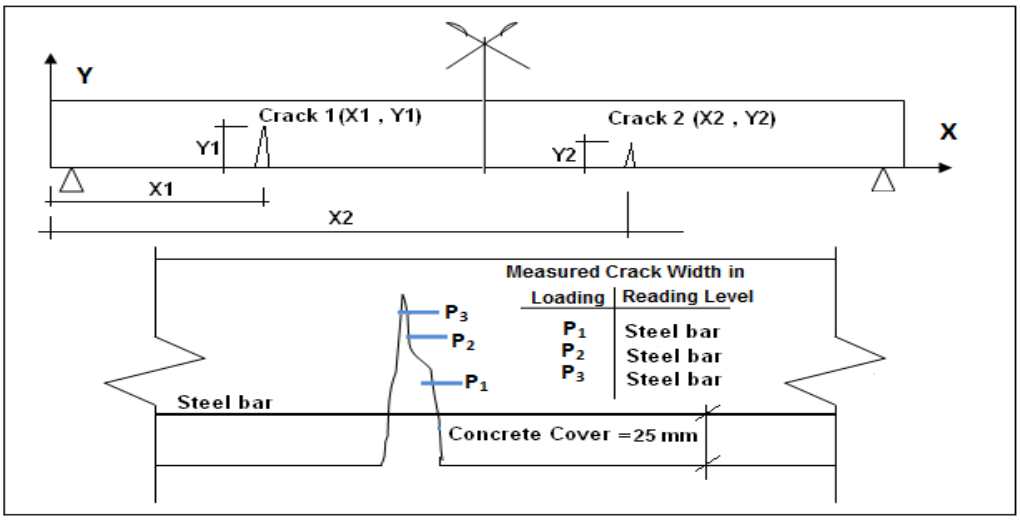

Figure 11. Measuring reference for the location and width provided in Tables 9–11 and Figure 8.

Table 9. Crack widths and their locations for the S512-1100 and S512-700 specimens.

S512-700				S512-1100			
Loading (kN)	**Location (mm)**		**Crack Width (mm)**	**Loading (kN)**	**Location (mm)**		**Crack Width (mm)**
	X	**Y**			**X**	**Y**	
24	580	35	0.20	20	710	35	0.20
24	710	40	0.15	21	1060	45	0.15
24	860	40	0.25	23	870	30	0.25
25	850	63	0.45	23	720	70	0.30
25	1160	35	0.20	23	1060	75	0.25
25	480	75	0.30	39	855	65	0.45
25	550	85	0.40	39	1060	80	0.50
28	700	70	0.30	39	735	85	0.55
28	1060	45	0.25	40	850	70	0.50
28	1140	65	0.40	40	1060	85	0.65
32	1040	60	0.30	42	1060	95	0.80
33	700	85	0.45	-	-	-	-
33	830	80	0.65	-	-	-	-
37	820	95	0.75	-	-	-	-
-	-	-	-	-	-	-	-

Table 10. Crack widths and their locations for the S512-1500 and S812-700 specimens.

S512-1500				S812-700			
Loading (kN)	**Location (mm)**		**Crack Width (mm)**	**Loading (kN)**	**Location (mm)**		**Crack Width (mm)**
	X	**Y**			**X**	**Y**	
20	1030	40	0.10	19.5	1220	35	0.25
20	850	30	0.15	25	640	25	0.15
21	700	25	0.25	25	730	20	0.20
21	850	50	0.20	25	1170	30	0.25
21	1050	50	0.15	25	1215	55	0.20
29	700	40	0.30	28	635	60	0.30
29	850	70	0.30	28	730	65	0.25
29	1030	65	0.25	32	640	70	0.32
29	1160	60	0.15	32	1170	45	0.45
32	600	20	0.25	32	1220	80	0.45
36	850	75	0.45	37	950	45	0.35
41	1140	85	0.45	37	1170	85	0.65
45.5	480	55	0.35	19.5	1220	35	0.25

Table 11. Crack widths and their locations for the S812-1100 and S812-1500 specimens.

S812-1100				S812-1500			
Loading (kN)	Location (mm)		Crack Width (mm)	Loading (kN)	Location (mm)		Crack Width (mm)
	X	Y			X	Y	
21	760	25	0.10	21	760	20	0.10
24	1040	10	0.15	21	1020	25	0.15
29	680	20	0.20	21.5	755	40	0.20
29	860	30	0.15	22	1035	30	0.25
29	1045	45	0.20	28	760	55	0.30
34	760	35	0.20	28	1045	60	0.30
34	860	40	0.25	29	860	25	0.15
34	1055	75	0.45	32	860	55	0.30
39	300	10	0.20	32	1055	80	0.40
39	630	40	0.25	39	610	35	0.10
39	775	75	0.50	40	1170	40	0.15
39	860	60	0.45	44	625	60	0.50
39	1140	35	0.10	44	860	85	0.55

5. Informational Model for Crack Width Prediction

5.1. ANN and Grey Wolf Optimization Algorithm

ANN is a computational model that simulates the practical features of biological neural networks [41]. As a parallel structure, an ANN consists of simple processing units similar to the human brain's structure, referred to as artificial neurons. The artificial neuron comprises bias, weights, and an activation function as per Equation (6), where f is the activation function, W_m is the weight matrix, X_m is the input vector, b is the bias vector, and Y is the output.

$$Y = f(\sum W_m X_m + b) \quad (6)$$

Grey wolves (which belong to the Canidae family) are recognized as apex predators located at the top of the food chain. In general, they live in packs with a group size of 5–12 with a strict community dominant hierarchy, as shown in Figure 12. The leaders are either female or male, and these so-called alphas (*a*, or leading wolf) principally make decisions regarding where/when to sleep, when to wake, and other activities, such as hunting. Every decision made by the *a* is fully dictated to the whole pack, though some cases of social behavior have also been observed, in which *a* may follow the other pack members. When they are near to each other, all of the group members admit the *a* as a leader by keeping their tails down. Only the *a* is allowed to mate in the pack. However, the *a* is not necessarily the strongest member, but rather the most skilled one in managing the group. In other words, the organization's discipline of the pack is of higher significance than the power of a group member.

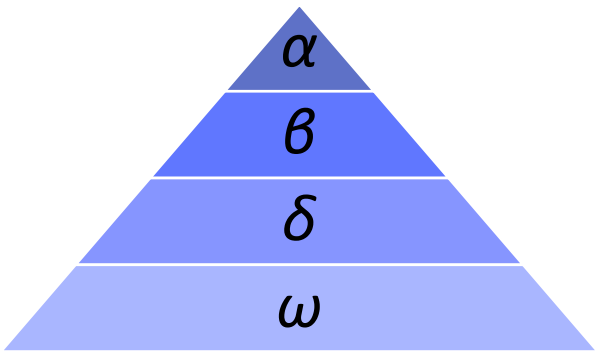

Figure 12. Grey wolves' hierarchy (supremacy declines from top to bottom).

In this hierarchy, the second level belongs to the beta, β, which is a subsidiary member that aids α in performing its activities and making decisions. The β can either be female or male and is possibly the most suitable candidate to be the α if one of the α wolves becomes very old or passes away. The β should obey the α, but commands the other wolves in the pack. β wolves play the role of a counselor to the α and a disciplinarian for the pack. The β reinforces the α's orders throughout the pack and advises the α.

The lowest position in the grey wolves' pack is the omega (ω). The ω is representative of a scapegoat, should always obey all of the other leading wolves, and comprises the wolves in the pack least allowed to eat. It may appear that the ω is not a group member; nevertheless, several observations have shown that the entire pack faces problems and internal fighting once losing the ω. It therefore helps to satisfy the whole pack and preserves the dominant structure.

In the case when a wolf is neither α nor β or ω, it is a subordinate (or delta, δ). δs obey α and β, but are still dominant over ωs. Sentinels, elders, hunters, caretakers, and scouts are categorized in this group. In general, scouts warn the pack when danger lies ahead and inspect the territory's boundaries, while sentinels defend the pack's safety. Elders are skilled wolves that have formerly been an α or β. Hunters assist the α and β in hunting and preparing food. Finally, caretakers care for the sick or weak members of the group. Furthermore, group hunting is another interesting aspect of the social hierarchy of a wolf' pack. The fundamental steps involved in grey wolves' hunting process have been summarized by Muro et al. [42] as follows: (i) chasing, tracking, and pursuing the prey; (ii) surrounding and harassing the prey until it stops running; and (iii) attacking the prey. Figure 13 illustrates all of these steps. Further information about the meta-heuristic Grey Wolf Optimizer can be found in [43], while the algorithm's performance in structural optimization problems compared to other metaheuristic algorithms has been studied in [44].

Figure 13. Hunting strategy of grey wolves: (**A**) chasing, approaching, and pursuing the prey, (**B**–**D**) pursuing, harassing, and surrounding, (**E**) inactive situation and attack [42] (with permission).

The steps of the optimization methodology using the Grey Wolf algorithm are shown in Figure 14. The iterations continue to find constant value as the stopping criteria, which are defined by the user. The objective function is the crack width of the one-way slab.

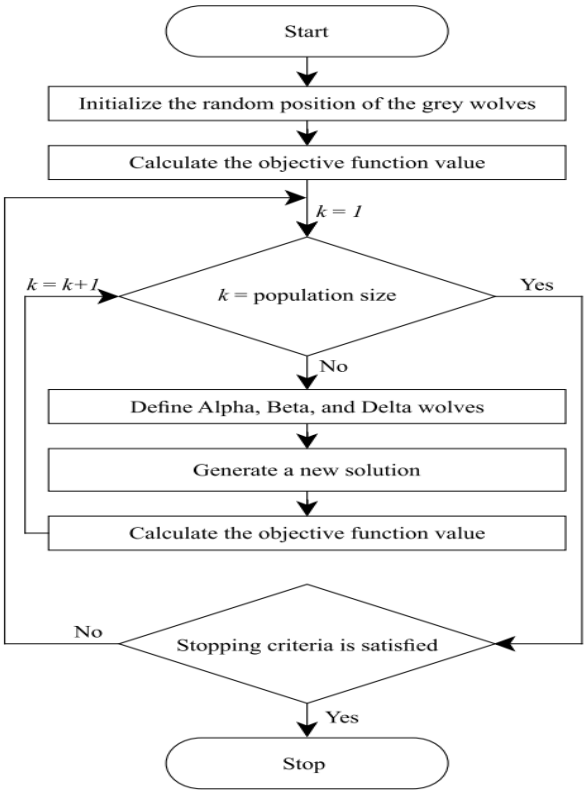

Figure 14. The Grey Wolf algorithm flowchart.

5.2. Generation of Training and Testing Data Sets

Table 12 illustrates the properties of the dataset used in this study, which is given in more detail in Appendix A. As mentioned earlier, the independent input parameters in each datum include the load magnitude, the ratio of the CFRP length to the slab bay, the ratio of the CFRP width to the slab bay, the crack location in the *x*-direction, the crack location in the *y*-direction, the stress in the steel bar, and the stress in the concrete, which form a 7 × 1 matrix, while the dependent output parameter is the crack width, which forms a 1 × 1 matrix. The data, including crack width, the stress in concrete and steel reinforcement, were generated at a given load for each specimen. Recording of the data began with the appearance of the first crack and continued until the ultimate capacity of the slab was reached.

Table 12. Properties of the used dataset.

Statistical Parameters	Unit	Type	Max	Min	STD	Average
Loading	(kN)	Input	54.0	19.5	8.3	31.4
CFRP Length/Slab Bay	-	Input	0.8	0.0	0.3	0.5
CFRP Width/Slab Width	-	Input	0.2	0.0	0.1	0.1
X Location	mm	Input	1385.0	300.0	233.1	870.5
Y Location	mm	Input	95.0	10.0	22.7	53.7
Stress in Steel Bar	MPa	Input	367.3	25.9	98.5	236.7
Stress in Concrete	MPa	Input	22.32	3.5	21.5	13.7
Crack Width	mm	Output	0.9	0.1	0.2	0.3

Any algebraic relationship, either causal or not, between two causal variables is known as the correlation or dependency. On a large scale, correlation denotes the degree to which a two or more variables are linearly correlated. A correlation matrix is a table presenting the relationship coefficients amongst the input variables where there is a correlation among the two parameters in each cell of the table. To analyze the data at an advanced level, a correlation matrix aids in summarizing the relationships between the data. The present paper's correlation matrix for the input/output parameters is displayed in Figure 15. Considering each input parameter's domain and evading any divergence in the results, Equation 7 was used to normalize each parameter in the range of −1 to 1, where X_n is the normalized value of the parameter, X_{max} is its maximum value, and X_{min} is its minimum value. X is the original (non-transformed) value of the variable.

$$X_n = \frac{2(X - X_{min})}{X_{max} - X_{min}} - 1 \quad (7)$$

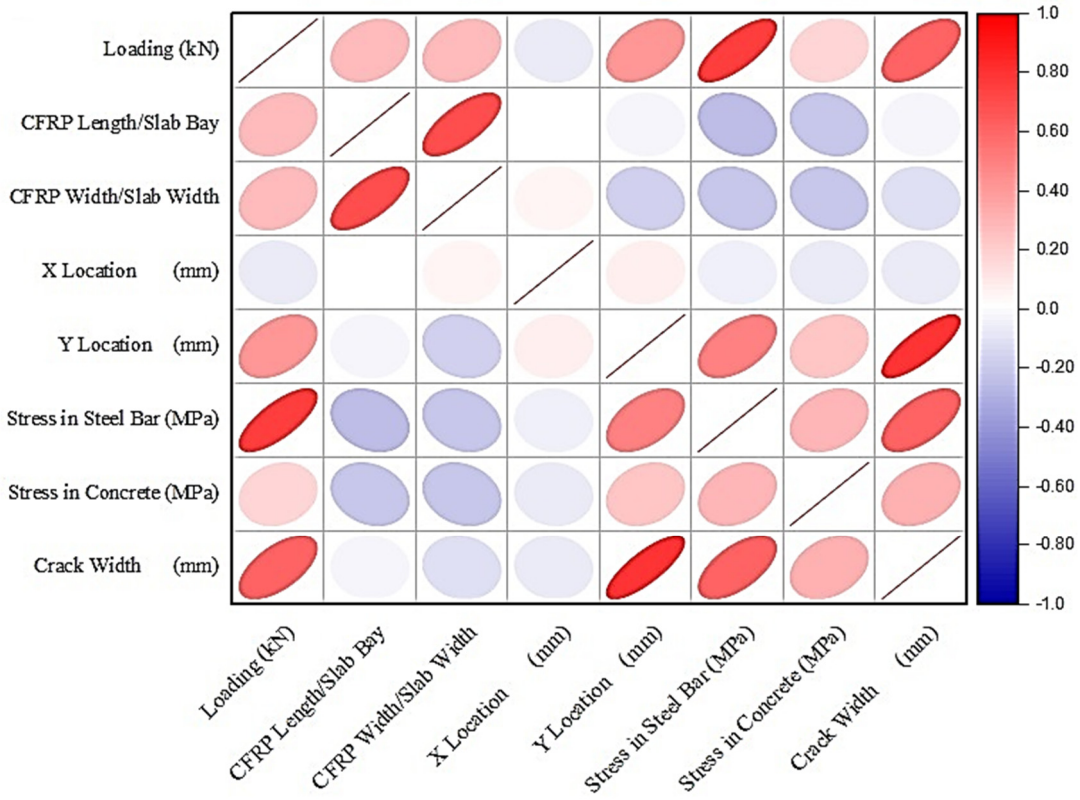

Figure 15. Correlation matrix between input and output parameters.

Figure 15 confirms that the output parameter, the crack width, mainly correlated with the depth of the beam (y location, stress in concrete and steel bars, and loading magnitude. Moreover, Figure 16 shows the histogram and half violin diagram of the output parameter.

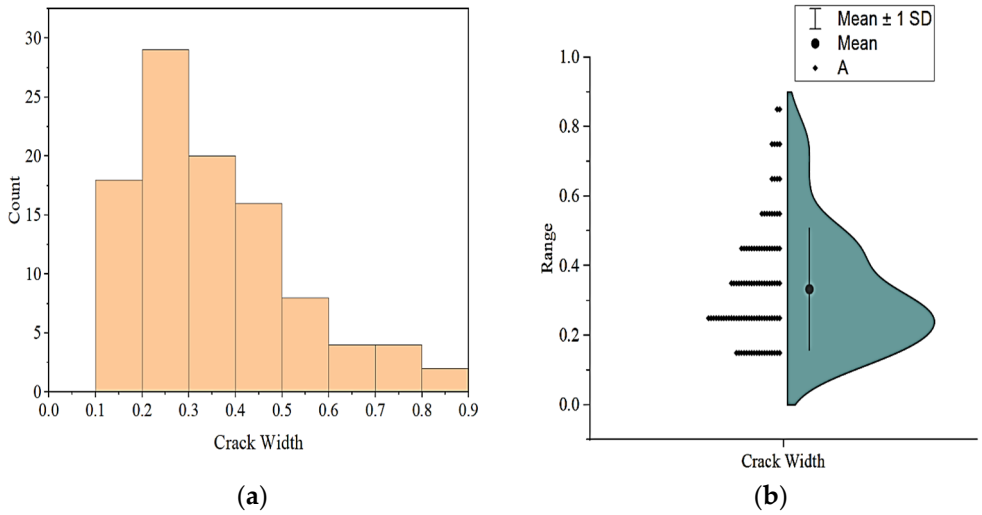

Figure 16. Output parameter crack width: (**a**) histogram and (**b**) half violin diagram.

The trial-and-error approach was adopted to develop the most effective architecture of the ANN model, which can best reproduce the features of the experimental dataset. In the present paper, an advanced technique was implemented for determining the number of neurons within the hidden layers based on Equation (8).

$$N_H \leq 2N_I + 1 \tag{8}$$

where N_H signifies the number of neurons within the hidden layers, and N_I stands for the number of input variables. The Levenberg–Marquardt training algorithm and hyperbolic tangent stimulation function were used in all developed networks. Moreover, the statistical indices, including the root mean squared error (*RMSE*), average absolute error (*AAE*), variance account factor (*VAF*), and correlation coefficient *R*, as expressed in Equations (9)–(12), were used to evaluate the performance of developed topologies.

$$RMSE = \left[\frac{1}{n}\sum_{i=1}^{n}(P_i - O_i)^2\right]^{\frac{1}{2}} \tag{9}$$

$$AAE = \frac{\left|\sum_{i=1}^{n}\frac{(O_i - P_i)}{O_i}\right|}{n} \times 100 \tag{10}$$

$$VAF = \left[1 - \frac{var(O_i - P_i)}{var(O_i)}\right] \times 100 \tag{11}$$

$$R = \left(\frac{\sum_{i=1}^{M}\left(y_{i(Actual)} - \overline{y}_{(Actual)}\right)\left(y_{i(Model)} - \overline{y}_{(Model)}\right)}{\sum_{i=1}^{M}\left(y_{i(Actual)} - \overline{y}_{(Actual)}\right)^2 \times \sum_{i=1}^{M}\left(y_{i(Model)} - \overline{y}_{(Model)}\right)}\right) \tag{12}$$

According to the number of input parameters, which is seven, Equation (8) resulted in 15 neurons within the hidden layers. Therefore, different architectures with two hidden layers and a maximum of 15 neurons in total were investigated. Overall, 30 different network topologies were evaluated. It was revealed that the network with a topology with 7-7-4-1 layers (two hidden layers) reached the lowest error values for *RMSE*, *AAE*, *VAF*, and the highest value of R^2 to estimate the crack width. Table 13 depicts the statistical metrics of selected topology which provided the most accurate results compared to the other two topologies. The ANN developed in this research was the *Newff* feedforward, where 70% of the dataset was considered for training, and the remaining 30% was used for testing the network. The Grey Wolf Optimizer (GWO) algorithm provided the least prediction error

for the trained structure and optimized both the biases and weights of the ANN. Table 14 shows the parameters of the employed GWO algorithm.

Table 13. Statistics of top three artificial neural networks combined Grey Wolf Optimizer on training and testing data.

Topology	Train			Test		
	RMSE	**AAE**	**VAF%**	**RMSE**	**AAE**	**VAF%**
GWO-ANN 2L(7-4)	0.05	0.15	91%	0.06	0.20	89%
GWO-ANN 2L(4-5)	0.08	0.24	78%	0.10	0.36	68%
GWO-ANN 2L(3-4)	0.06	0.19	86%	0.09	0.29	77%

Table 14. Parameters of the GWO algorithm.

Parameter	Value
Max generations	300
Search agents	10

5.3. Multiple Linear Regression and Imperialist Competitive Algorithm Models

To examine the reliability of the proposed hybrid GWO-ANN model, a multiple linear regression (MLR) model was also developed in this research. In the MLR model, some independent parameters mainly influence the dependent variable, as per Equation (10), where y is a dependent or output parameter and x_1, x_2, ... are independent input parameters. $a_1, a_2, \ldots$ are coefficients of the equation.

$$y = f(x_1, x_2, \ldots) \rightarrow y = a_0 + a_1 x_1 + a_2 x_2 + \ldots \tag{13}$$

Equation (11) shows the most appropriate coefficients for the MLR model for estimating the studied specimens' crack width, and Table 15 depicts the statistical metrics resulting from this model.

$$\begin{aligned} Crack\ Width = \quad & -0.0957 + 0.00839 Loading \\ & -0.0757 CFRP\ Length/Slab\ Bay \\ & -0.030 CFRP\ Width/Slab\ Width - 0.000049 X\ Location \\ & +0.00503 Y\ Location - 0.000119 Stress\ in\ Steel\ Bar \\ & +0.000692\ Stress\ in\ Concrete \end{aligned} \tag{14}$$

Table 15. Statistical metrics resulting from MLR model.

Topology	Train			Test		
	RMSE	**AAE**	**VAF%**	**RMSE**	**AAE**	**VAF%**
MLR	0.08	0.24	76%	0.09	0.32	74%

5.4. Comparison of Accuracy of Proposed GWO-ANN Model

Figures 17 and 18 compare the actual experimental data with the predictions of the novel GWO-ANN computational intelligence model developed in this study and the MLR model. It can be observed that the GWO-ANN performed more reliably in estimating the crack width compared to the MLR informational models.

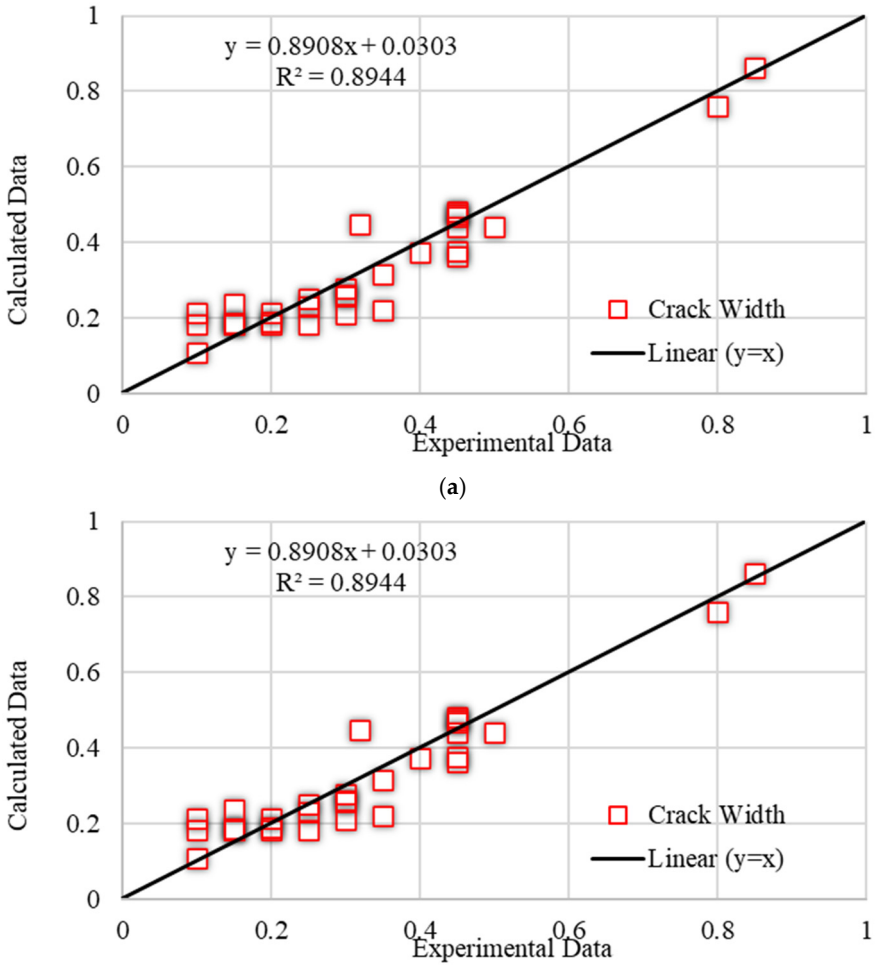

Figure 17. Experimental versus predicted values for estimating crack width using GWO-ANN: (**a**) Training data, (**b**) Testing data.

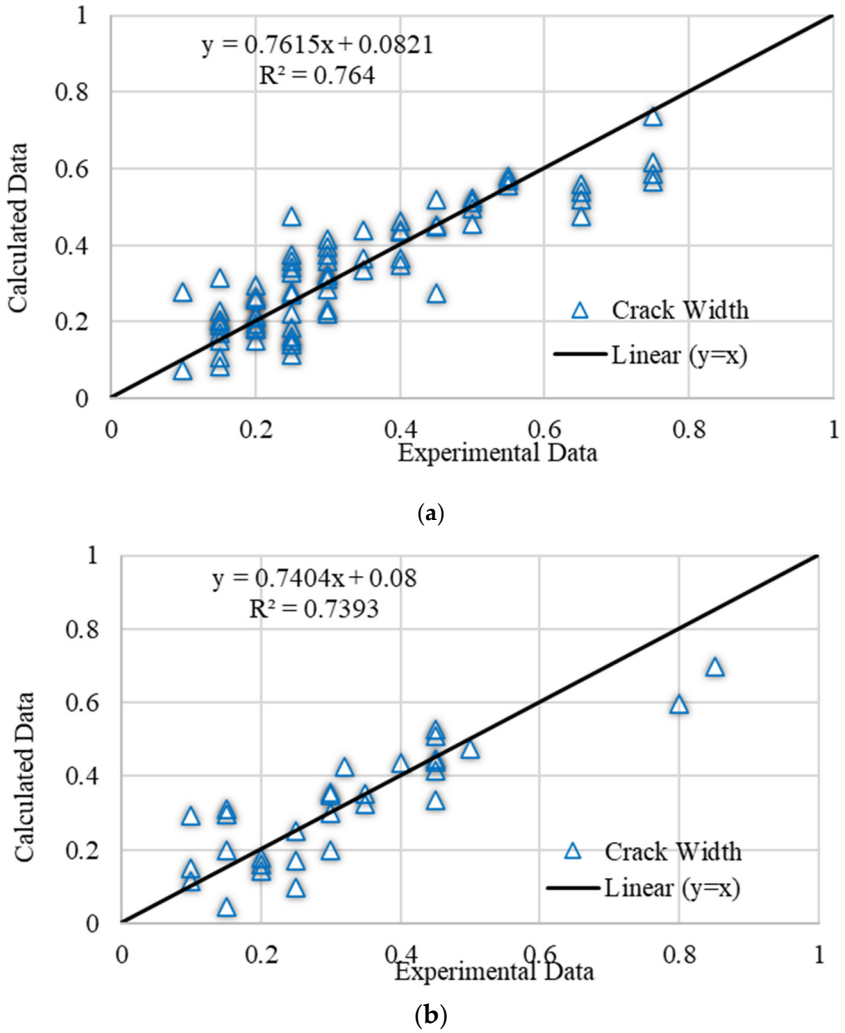

Figure 18. Experimental versus predicted values for predicting crack width using MLR: (**a**) Training data, (**b**) Testing data.

6. Conclusions

This research work examines the effects of carbon fiber-reinforced polymer (CFRP) strengthening on the crack development in reinforced concrete slabs and develops an informational model using a hybrid Grey Wolf Optimizer-Artificial Neural Network algorithm (GWO-ANN) to estimate the crack width. Six reinforced concrete (RC) slabs strengthened with CFRP of various lengths were tested, and the results were compared to those of conventional RC slabs. Applied loading, CFRP width/length, X/Y crack positions, and steel reinforcement and concrete stress were defined as the input parameters for the development of the informational model. The main findings of the research work are summarized below:

- Before steel reinforcement's yielding, the CFRP plate was de-bonded at the CFRP/concrete contact.
- EC2 provides an unconservative estimation for the RC slabs' crack widths when CFRP laminates are attached to the slab for strengthening purposes. This behavior can be explained by the fact that attaching the CFRP laminates to the RC slabs leads to increased stiffness and bending moment capacity of the section, which is not accounted for by the EC2 formulas and may be associated with the unconservative estimation for the crack widths.

- On average, the crack width in slabs retrofitted with CFRP laminates increased by around 80% compared to a slab without CFRP. Nevertheless, increasing the length and width of CFRP laminates had a minor effect on strength and crack development.
- The results confirm the higher reliability of the proposed GWO-ANN model for estimating the crack width in flat slabs compared to the multiple linear regression (MLR) model. The statistical metrics used, namely RMSE, AAE, and VAF, showed the better performance of the proposed GWO-ANN model in comparison with the MLR model. It captures the underlying mechanisms involved in the crack development of the slab. Accordingly, the proposed equation developed using the MLR model can be directly used without time-consuming analysis and computations. This empirical expression is primarily a function of the slab/CFRP geometry and the crack location.

Author Contributions: Conceptualization, S.V.R.T., I.F. and M.L.N.; methodology, I.F., M.L.N. and V.P.; software, M.L.N., V.P. and K.A.V.; validation, V.P., K.A.V. and S.V.R.T.; formal analysis, S.V.R.T., I.F. and M.L.N.; investigation, I.F., M.L.N. and V.P.; resources, K.A.V., S.V.R.T. and I.F.; data curation, K.A.V., S.V.R.T. and I.F.; writing—original draft preparation, S.V.R.T., I.F. and M.L.N.; writing—review and editing, I.F., M.L.N. and V.P.; visualization, V.P., K.A.V. and S.V.R.T.; supervision, M.L.N. and V.P.; project administration, M.L.N., V.P. and K.A.V. All authors have read and agreed to the published version of the manuscript.

Funding: This research received no external funding.

Data Availability Statement: Data used for model development are provided in the Appendix A. The corresponding author can provide any other details of this study upon request.

Conflicts of Interest: The authors declare no conflict of interest.

Appendix A

Table A1. The dataset used in this study.

	Input Parameters							Output
ID	**Loading (kN)**	**CFRP Length/Slab Bay**	**CFRP Width/Slab Width**	**X Location (mm)**	**Y Location (mm)**	**Steel Bar Stress (MPa)**	**Concrete Stress (MPa)**	**Crack Width (mm)**
1	24	0.388	0.1	580	35	142.5	8.269	0.2
2	24	0.388	0.1	710	40	142.5	8.269	0.15
3	24	0.388	0.1	860	40	142.5	8.269	0.25
4	25	0.388	0.1	850	63	227.4	9.17	0.45
5	25	0.388	0.1	1160	35	227.4	9.17	0.2
6	25	0.388	0.1	480	75	227.4	9.17	0.3
7	25	0.388	0.1	550	85	227.4	9.17	0.4
8	28	0.388	0.1	700	70	303	10.466	0.3
9	28	0.388	0.1	1060	45	303	10.466	0.25
10	28	0.388	0.1	1140	65	303	10.466	0.4
11	32	0.388	0.1	1040	60	340	10.81	0.3
12	33	0.388	0.1	700	85	351	11.11	0.45
13	33	0.388	0.1	830	80	351	11.11	0.65
14	37	0.388	0.1	820	95	359	13.82	0.75
15	20	0.61	0.1	710	35	67.42	6.88	0.2
16	21	0.61	0.1	1060	45	107.5	7.44	0.15
17	23	0.61	0.1	870	30	167.7	8.01	0.25
18	23	0.61	0.1	720	70	167.7	8.01	0.3
19	23	0.61	0.1	1060	75	167.7	8.01	0.25
20	39	0.61	0.1	855	65	215	9.13	0.45

Table A1. *Cont.*

	Input Parameters							Output
ID	**Loading (kN)**	**CFRP Length/Slab Bay**	**CFRP Width/Slab Width**	**X Location (mm)**	**Y Location (mm)**	**Steel Bar Stress (MPa)**	**Concrete Stress (MPa)**	**Crack Width (mm)**
21	39	0.61	0.1	1060	80	215	9.13	0.5
22	39	0.61	0.1	735	85	215	9.13	0.55
23	40	0.61	0.1	850	70	276.3	10.53	0.5
24	40	0.61	0.1	1060	85	276.3	10.53	0.65
25	42	0.61	0.1	1060	95	366	10.91	0.8
26	20	0.83	0.1	1030	40	92.27	5.19	0.1
27	20	0.83	0.1	850	30	92.27	5.19	0.15
28	21	0.83	0.1	700	25	118.4	6.1	0.25
29	21	0.83	0.1	850	50	118.4	6.1	0.2
30	21	0.83	0.1	1050	50	118.4	6.1	0.15
31	29	0.83	0.1	700	40	187	8.69	0.3
32	29	0.83	0.1	850	70	187	8.69	0.3
33	29	0.83	0.1	1030	65	187	8.69	0.25
34	29	0.83	0.1	1160	60	187	8.69	0.15
35	32	0.83	0.1	600	20	210.7	9.35	0.25
36	36	0.83	0.1	850	75	251.26	10.38	0.45
37	41	0.83	0.1	1140	85	289.3	11.94	0.45
38	45.5	0.83	0.1	480	55	363.35	14.41	0.35
39	45.5	0.83	0.1	690	85	363.35	14.41	0.55
40	45.5	0.83	0.1	1000	85	363.35	14.41	0.75
41	19.5	0.388	0.16	1220	35	25.88	3.51	0.25
42	25	0.388	0.16	640	25	51.77	5.73	0.15
43	25	0.388	0.16	730	20	51.77	5.73	0.2
44	25	0.388	0.16	1170	30	51.77	5.73	0.25
45	25	0.388	0.16	1215	55	51.77	5.73	0.2
46	28	0.388	0.16	635	60	214.48	7.55	0.3
47	28	0.388	0.16	730	65	214.48	7.55	0.25
48	32	0.388	0.16	640	70	340.2	11.71	0.32
49	32	0.388	0.16	1170	45	340.2	11.71	0.45
50	32	0.388	0.16	1220	80	340.2	11.71	0.45
51	37	0.388	0.16	950	45	356	22.1	0.35
52	37	0.388	0.16	1170	85	356		0.65
53	21	0.61	0.16	760	25	72.5	7.86	0.1
54	24	0.61	0.16	1040	10	121	9.21	0.15
55	29	0.61	0.16	680	20	176.6	11.42	0.2
56	29	0.61	0.16	860	30	176.6	11.42	0.15
57	29	0.61	0.16	1045	45	176.6	11.42	0.2
58	34	0.61	0.16	760	35	239	13.51	0.2
59	34	0.61	0.16	860	40	239	13.51	0.25
60	34	0.61	0.16	1055	75	288	13.51	0.45
61	39	0.61	0.16	300	10	288	15.84	0.2
62	39	0.61	0.16	630	40	288	15.84	0.25
63	39	0.61	0.16	775	75	288	15.84	0.5
64	39	0.61	0.16	860	60	288	15.84	0.45
65	39	0.61	0.16	1140	35	288	15.84	0.1
66	39	0.61	0.16	1385	45	288	15.84	0.15
67	45	0.61	0.16	300	20	358.8	15.84	0.3
68	45	0.61	0.16	600	20	358.8	18.18	0.25
69	45	0.61	0.16	650	70	358.8	18.18	0.5
70	45	0.61	0.16	790	90	358.8	18.18	0.75
71	45	0.61	0.16	1245	25	358.8	18.18	0.2
72	45	0.61	0.16	1385	60	358.8	18.18	0.4
73	21	0.83	0.16	760	20	75.7	6.83	0.1

Table A1. *Cont.*

	Input Parameters							Output
ID	**Loading (kN)**	**CFRP Length/Slab Bay**	**CFRP Width/Slab Width**	**X Location (mm)**	**Y Location (mm)**	**Steel Bar Stress (MPa)**	**Concrete Stress (MPa)**	**Crack Width (mm)**
74	21	0.83	0.16	1020	25	75.7	6.83	0.15
75	21.5	0.83	0.16	755	40	85.3	7.77	0.2
76	22	0.83	0.16	1035	30	115.8	9.38	0.25
77	28	0.83	0.16	760	55	149.7	10.45	0.3
78	28	0.83	0.16	1045	60	149.7	10.45	0.3
79	29	0.83	0.16	860	25	187.8	12.19	0.15
80	32	0.83	0.16	860	55	222.2	13.39	0.3
81	32	0.83	0.16	1055	80	222.2	13.39	0.4
82	39	0.83	0.16	610	35	222.2	14.6	0.1
83	40	0.83	0.16	1170	40	249	15.2	0.15
87	44	0.83	0.16	625	60	288	16.61	0.5
85	44	0.83	0.16	860	85	288	16.61	0.55
86	48	0.83	0.16	640	75	321	18.1	0.65
87	54	0.83	0.16	860	95	363	20.76	0.85
88	21	0	0	640	30	191	9.21	0.25
89	21	0	0	760	34	191	9.21	0.3
90	21	0	0	980	41	191	9.21	0.3
91	23	0	0	750	62	222	10.21	0.35
92	24	0	0	647	54	258	11.18	0.3
93	24	0	0	990	66	258	11.18	0.35
94	24	0	0	1100	35	298.8	13.21	0.15
95	26	0	0	1285	30	321.2	15.41	0.2
96	33	0	0	680	80	362	18.21	0.45
97	33	0	0	1080	75	362	18.21	0.25
98	33	0	0	1270	55	362	18.21	0.4
99	33	0	0	590	40	362	18.21	0.35
100	33	0	0	380	60	362	18.21	0.4
101	33.3	0	0	740	95	367.3	223.2	0.75

References

1. Nawy, E.G.; Orenstein, G.S. Crack width control in reinforced concrete two-way slabs. *J. Struct. Div.* **1970**, *96*, 701–721. [CrossRef]
2. Nawy, E.G. *Reinforced Concrete*; Prentice-Hall: Hoboken, NJ, USA, 1985; ISBN 0137716435.
3. Baumann, R.A.; Weisgerber, F.E. Yield-line analysis of slabs-on-grade. *J. Struct. Eng.* **1983**, *109*, 1553–1568. [CrossRef]
4. Ross, T.J.; Krawinkler, H. Impulsive direct shear failure in RC slabs. *J. Struct. Eng.* **1985**, *111*, 1661–1677. [CrossRef]
5. Park, R.; Gamble, W.L. *Reinforced Concrete Slabs*; John Wiley & Sons: Hoboken, NJ, USA, 1999; ISBN 0471348503.
6. Gergely, P.; Lutz, L.A. Maximum crack width in reinforced concrete flexural members. *Spec. Publ.* **1968**, *20*, 87–117.
7. *EN 1992-1-1*; Eurocode 2: Design of Concrete Structures—Part 1. British Standard Institution: London, UK, 2004.
8. Mosallam, A.S.; Mosalam, K.M. Strengthening of two-way concrete slabs with FRP composite laminates. *Constr. Build. Mater.* **2003**, *17*, 43–54. [CrossRef]
9. El Maaddawy, T.; Soudki, K. Strengthening of reinforced concrete slabs with mechanically-anchored unbonded FRP system. *Constr. Build. Mater.* **2008**, *22*, 444–455. [CrossRef]
10. Zheng, X.; Wan, B.; Huang, P.; Huang, J. Experimental study of hybrid strengthening technique using carbon fiber laminates and steel plates for reinforced concrete slabs. *Constr. Build. Mater.* **2019**, *210*, 324–337. [CrossRef]
11. Chen, C.-C.; Chen, S.-L. Strengthening of reinforced concrete slab-column connections with carbon fiber reinforced polymer laminates. *Appl. Sci.* **2020**, *10*, 265. [CrossRef]
12. Duxson, P.; Provis, J.L.; Lukey, G.C.; Van Deventer, J.S. The role of inorganic polymer technology in the development of 'green concrete'. *Cem. Concr. Res.* **2007**, *37*, 1590–1597. [CrossRef]
13. Naser, M.; Hawileh, R.; Abdalla, J. Fiber-reinforced polymer composites in strengthening reinforced concrete structures: A critical review. *Eng. Struct.* **2019**, *198*, 109542. [CrossRef]
14. Abiodun, O.I.; Jantan, A.; Omolara, A.E.; Dada, K.V.; Mohamed, N.A.; Arshad, H. State-of-the-art in artificial neural network applications: A survey. *Heliyon* **2018**, *4*, e00938. [CrossRef] [PubMed]
15. Pan, Y.; Zhang, L. Roles of artificial intelligence in construction engineering and management: A critical review and future trends. *Autom. Constr.* **2021**, *122*, 103517. [CrossRef]

16. Lagaros, N.D.; Plevris, V. Artificial Intelligence (AI) Applied in Civil Engineering. *Appl. Sci.* **2022**, *12*, 7595. [CrossRef]
17. Mangalathu, S.; Shin, H.; Choi, E.; Jeon, J.-S. Explainable machine learning models for punching shear strength estimation of flat slabs without transverse reinforcement. *J. Build. Eng.* **2021**, *39*, 102300. [CrossRef]
18. Lagaros, N.D.; Papadrakakis, M. Learning improvement of neural networks used in structural optimization. *Adv. Eng. Soft.* **2004**, *35*, 9–25. [CrossRef]
19. Plevris, V.; Tsiatas, G. Computational Structural Engineering: Past Achievements and Future Challenges. *Front. Built Environ.* **2018**, *4*, 21. [CrossRef]
20. Kandiri, A.; Sartipi, F.; Kioumarsi, M. Predicting Compressive Strength of Concrete Containing Recycled Aggregate Using Modified ANN with Different Optimization Algorithms. *Appl. Sci.* **2021**, *11*, 485. [CrossRef]
21. Dabiri, H.; Kioumarsi, M.; Kheyroddin, A.; Kandiri, A.; Sartipi, F. Compressive strength of concrete with recycled aggregate; a machine learning-based evaluation. *Clean. Mater.* **2022**, *3*, 100044. [CrossRef]
22. Waris, M.I.; Mir, J.; Plevris, V.; Ahmad, A. Predicting compressive strength of CRM samples using Image processing and ANN. *IOP Conf. Ser. Mater. Sci. Eng.* **2020**, *899*, 012014. [CrossRef]
23. Ahmadi, M.; Kheyroddin, A.; Dalvand, A.; Kioumarsi, M. New empirical approach for determining nominal shear capacity of steel fiber reinforced concrete beams. *Constr. Build. Mater.* **2020**, *234*, 117293. [CrossRef]
24. Sharib, S.; Ahmad, N.; Plevris, V.; Ahmad, A. Prediction Models for Load Carrying Capacity of RC Wall through Neural Network. In Proceedings of the 14th ECCOMAS Thematic Conference on Evolutionary and Deterministic Methods for Design, Optimization and Control (EUROGEN 2021), 2021, ECCOMAS, Athens, Greece, 28–30 June 2021; pp. 132–142. [CrossRef]
25. Yaseen, Z.M.; Deo, R.C.; Hilal, A.; Abd, A.M.; Bueno, L.C.; Salcedo-Sanz, S.; Nehdi, M.L. Predicting compressive strength of lightweight foamed concrete using extreme learning machine model. *Adv. Eng. Soft.* **2018**, *115*, 112–125. [CrossRef]
26. Ahmad, A.; Plevris, V.; Khan, Q.-u.-Z. Prediction of Properties of FRP-Confined Concrete Cylinders Based on Artificial Neural Networks. *Crystals* **2020**, *10*, 811. [CrossRef]
27. Solorzano, G.; Plevris, V. Design of Reinforced Concrete Isolated Footings under Axial Loading with Artificial Neural networks. In Proceedings of the 14th ECCOMAS Thematic Conference on Evolutionary and Deterministic Methods for Design, Optimization and Control (EUROGEN 2021), Athens, Greece, 28–30 June 2021; pp. 118–131.
28. Papadrakakis, M.; Papadopoulos, V.; Lagaros, N.D.; Oliver, J.; Huespe, A.E.; Sanchez, P. Vulnerability analysis of large concrete dams using the continuum strong discontinuity approach and neural networks. *Struct. Saf.* **2008**, *30*, 217–235. [CrossRef]
29. Imran Waris, M.; Plevris, V.; Mir, J.; Chairman, N.; Ahmad, A. An alternative approach for measuring the mechanical properties of hybrid concrete through image processing and machine learning. *Constr. Build. Mater.* **2022**, *328*, 126899. [CrossRef]
30. Faridmehr, I.; Shariq, M.; Plevris, V.; Aalimahmoody, N. Novel hybrid informational model for predicting the creep and shrinkage deflection of reinforced concrete beams containing GGBFS. *Neural Comput. Appl.* **2022**, *34*, 13107–13123. [CrossRef]
31. Ben Seghier, M.E.A.; Corriea, J.A.F.O.; Jafari-Asl, J.; Malekjafarian, A.; Plevris, V.; Trung, N.-T. On the modeling of the annual corrosion rate in main cables of suspension bridges using combined soft computing model and a novel nature-inspired algorithm. *Neural Comput. Appl.* **2021**, *33*, 15969–15985. [CrossRef]
32. Asteris, P.G.; Plevris, V. Neural Network approximation of the masonry failure under biaxial compressive stress. In Proceedings of the 3rd South-East European Conference on Computational Mechanics (SEECCM III), Kos Island, Greece, 12–14 June 2013; pp. 584–598.
33. Menna, D.W.; Genikomsou, A.S. Punching Shear Response of Concrete Slabs Strengthened with Ultrahigh-Performance Fiber-Reinforced Concrete Using Finite-Element Methods. *Pract. Period. Struct. Des. Constr.* **2021**, *26*, 04020057. [CrossRef]
34. Torabian, A.; Isufi, B.; Mostofinejad, D.; Ramos, A.P. Flexural strengthening of flat slabs with FRP composites using EBR and EBROG methods. *Eng. Struct.* **2020**, *211*, 110483. [CrossRef]
35. Chalot, A.; Roy, N.; Michel, L.; Ferrier, E. Mechanical behavior of a full-scale RC wall-slab connection reinforced with frp under cyclic loading. *Eng. Struct.* **2021**, *239*, 112146. [CrossRef]
36. Beeby, A.W.; Narayanan, R.S.; Narayanan, R. *Designers' Handbook to Eurocode 2: Design of Concrete Structures*; Thomas Telford: London, UK, 1995; ISBN 0727716689.
37. Bye, G.C. *Portland Cement: Composition, Production and Properties*; Thomas Telford: London, UK, 1999; ISBN 0727727664.
38. *Bsi, B. 8110-1*; Structural Use of Concrete, Code of Practice for Design and Construction, Part 1. British Standard Institution: London, UK, 1997.
39. Clarke, J.; Waldron, P. The reinforcement of concrete structures with advanced composites. *Struct. Eng.* **1996**, *74*, 283–288.
40. Teychenne, D.; Franklin, R.; Erntroy, H. *Design of Normal Concrete Mixes*; Department of the Environment: London, UK, 1975.
41. Agatonovic-Kustrin, S.; Beresford, R. Basic concepts of artificial neural network (ANN) modeling and its application in pharmaceutical research. *J. Pharm. Biomed. Anal.* **2000**, *22*, 717–727. [CrossRef]
42. Muro, C.; Escobedo, R.; Spector, L.; Coppinger, R. Wolf-pack (Canis lupus) hunting strategies emerge from simple rules in computational simulations. *Behav. Process.* **2011**, *88*, 192–197. [CrossRef] [PubMed]
43. Mirjalili, S.; Mirjalili, S.M.; Lewis, A. Grey Wolf Optimizer. *Adv. Eng. Soft.* **2014**, *69*, 46–61. [CrossRef]
44. Lagaros, N.D.; Plevris, V.; Kallioras, N.A. The Mosaic of Metaheuristic Algorithms in Structural Optimization. *Arch. Comput. Methods Eng.* **2022**. [CrossRef]